BACKSCATTER

The scattering of waves from an object is a diffraction process that transforms the incident wave into the waves propagating from the object in all possible directions. The *backscatter,* or *backscattering,* is the scattering of waves back toward the source of the incident wave. This process substantially depends on material properties of the scattering object, its shape, size, and spatial orientation relative to the incident wave, as well as on the frequency and polarization of the incident wave. One distinguishes three frequency regions with different physical properties of scattered waves. They are quasi-static, resonance, and quasi-optical regions.

QUASI-STATIC SCATTERING

In the quasi-static region (sometimes called the Rayleigh region), the wavelength λ of the incident wave is much greater than the maximum linear dimension l of the scattering object ($\lambda \gg l$). At a certain time t, the scattered field at small distances ($r \ll \lambda$) from the object is approximately the static field created by dipoles and multipoles induced by the incident wave in the scattering object at the same time t. Far from the object, the scattered field is an outgoing spherical wave. Its average power flux density (over one period of oscillations) relative to that of the incident wave, or radar cross-section (RCS), is determined by the object's volume rather than the shape of the object, and it is proportional to λ^{-4}. Specifically, this dependence explains the blue color of the cloudless sky during the day. This color is due to the predominance of blue light scattered by small inhomogeneities of the air caused by fluctuations of its density. The violet light, which is shorter in wavelength, undergoes stronger relative scattering and as a result suffers higher attenuation while propagating through the atmosphere. Analytical expressions for quasi-static RCS of some scattering objects can be found in (1–3). For example, the axial RCS of perfectly conducting bodies of revolution is determined by the following approximation (p. 145 of Ref. 1):

$$\sigma \approx \frac{4}{\pi} k^4 V^2 \cdot \left(1 + \frac{e^{-\tau}}{\pi\tau}\right)^2 \tag{1}$$

where $k = 2\pi/\lambda$ is the wave number, V is the object's volume, and τ is the characteristic length-to-width ratio of the object. This quantity τ is found for each object's shape by allowing the axial dimension of the object to go to zero so as to obtain the correct result

$$\sigma = \frac{64}{9\pi} k^4 a^6 \tag{2}$$

for the circular disk with radius a. Table 8.2 in Ref. 2 (Vol. 2, pp. 558–561) contains explicit expressions for RCS found in this manner for a variety of bodies of revolution. The first term in this table (Eq. 8.1-87a on p. 558) contains a misprint. The letter b should be replaced by h.

In this frequency region, the scattered field can be expressed in terms of a convergent series in positive integer power of the wave number $k = 2\pi/\lambda$. The expansion coefficients are found from the solution of the recursive system of boundary value problems in potential theory (pp. 848–856 of Ref. 4). In practice it is possible to find only a few first coefficients. Direct numerical methods are efficient tools for the solution of quasi-static scattering problems (5–7).

RESONANCE SCATTERING

In the resonance frequency region, linear dimensions of scattering objects are comparable to the wavelength of the incident wave. Eigen-oscillations excited by the incident wave in the scattering object can substantially influence the scattering property. Frequencies of these oscillations are complex quantities. Their imaginary parts determine both the internal (thermal) losses inside the object and the external losses that are due to radiation into the surrounding medium. A major contribution to RCS is given by the radiation of those eigen-oscillations, whose eigenfrequency real part and polarization are close to the incident wave frequency and polarization. If the quality factor of these oscillations is quite large, the amplitude and the intensity of the scattered wave sharply increase as the frequency of the incident wave approaches the real part of the frequency of eigen-oscillations. This phenomenon is referred to as "resonance scattering." It reveals itself, for example, in scatterings from thin metallic half-wavelength long wires and narrow strips (pp. 293–303 of Ref. 2). These scatterers are used, in particular, to create a chaff clutter for radars. Analytical and numerical data for scattering by thin wires are collected in chapter 12 of Ref. 3. Recent analytical results for resistive wires are presented in Ref. 8.

The resonance scattering from wires can also be explained as being due to the constructive interference of multiple current waves arising from the wire ends. This process is investigated in detail in Ref. 9. The total current generated by the incident plane wave in the perfectly conducting wire (Fig. 1) equals

$$J(z) = J_0(z) + \sum_{n=1}^{\infty} [J_n^+(z) + J_n^-(z)] \tag{3}$$

with the time dependence $\exp(-i\omega t)$ assumed and suppressed here and later. The term $J_0(z)$ is the current induced by the incident wave in the infinitely long wire ($-\infty \le z \le +\infty$). The terms $J_n^+(z)$ and $J_n^-(z)$ are multiple current waves. Waves $J_n^+(z)$ run in the positive z-direction from the left wire end $z = -l$ to the right end $z = +l$. Waves $J_n^-(z)$ run in the negative z-direction from the right end $z = +l$ to the left end $z = -l$. The total length of the wire is $L = 2l$. When the wave $J_n^{\pm}(z)$ reaches the opposite end it undergoes diffraction and transforms into the wave $J_{n+1}^{\mp}(z)$. At the end points of the wire the total current and its components satisfy the conditions

$$J(\pm l) = 0, \qquad J_1^+(-l) = -J_0(-l), \qquad J_1^-(l) = -J_0(l) \tag{4}$$

$$J_{n+1}^+(-l) = -J_n^-(-l), \qquad J_{n+1}^-(l) = -J_n^+(l), \qquad n = 1, 2, 3, \ldots \tag{5}$$

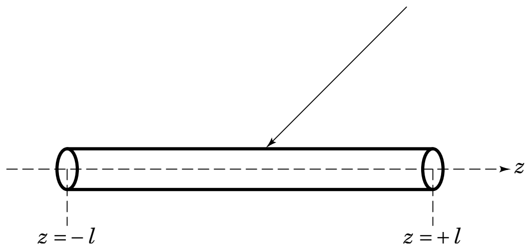

Figure 1. A thin wire excited by an incident wave. The radius of the wire is small compared with the wavelength. Such a wire can support traveling waves due to the multiple edge diffractions. A constructive interference of these waves results in the resonance behavior of the surface current and scattered field.

In thin wires ($ka < 0.2$, a is the wire radius), the multiple current waves are described by the following approximate expressions

$$\begin{aligned} J_{2n}^{+}(z) &= -J_1^{-}(-l)[\psi(kL)e^{ikL}]^{2n-2}\psi[k(l+z)]e^{ik(l+z)} \\ J_{2n+1}^{+}(z) &= J_1^{+}(l)[\psi(kL)e^{ikL}]^{2n-1}\psi[k(l+z)]e^{ik(l+z)} \\ J_{2n}^{-}(z) &= -J_1^{+}(l)[\psi(kL)e^{ikL}]^{2n-2}\psi[k(l-z)]e^{ik(l-z)} \\ J_{2n+1}^{-}(z) &= J_1^{-}(-l)[\psi(kL)e^{ikL}]^{2n-1}\psi[k(l-z)]e^{ik(l-z)} \end{aligned} \quad (6)$$

with $n = 1, 2, 3, \ldots$. Function $\psi(kz)$ is defined in (10) as

$$\psi(kz) = \frac{2\ln\dfrac{i}{\gamma ka}}{\ln\dfrac{2ikz}{\gamma q} - \mathrm{E}(2kz)e^{-2ikz}} \quad (7)$$

where

$$q = (ka)^2, \qquad \gamma = 1.781\ldots, \qquad \ln(i) = i\pi/2$$

and

$$\mathrm{E}(x) = -\int_x^\infty \frac{e^{it}}{t}\,dt = \mathrm{Ci}(x) + i\mathrm{Si}(x) \quad (8)$$

Functions $\mathrm{Ci}(x)$ and $\mathrm{Si}(x)$ are the well-tabulated cosine and sine integrals, respectively. For small arguments ($x \ll 1$), function $\mathrm{E}(x)$ reduces to $\mathrm{E}(x) = \ln(\gamma x) - \ln(i) + O(x)$ and ensures the equality $\psi(0) = 1$. Equation (6) shows that all multiple edge waves starting with secondary waves ($n = 2, 3, 4, \ldots$) are expressed approximately by the same function $\psi(x)$. As a result, the substitution of expressions (6) into Eq. (3) leads to the geometric series

$$\begin{aligned} \sum_{n=2}^{\infty}[J_n^{+}(z) + J_n^{-}(z)] &= f(k,z,l,a)\sum_{m=0}^{\infty}\{[\psi(kL)e^{ikL}]^2\}^m \\ &= \frac{f(k,z,l,a)}{D} \end{aligned} \quad (9)$$

which contains the resonance denominator $D(ka, kL) = 1 - [\psi(kL)e^{ikL}]^2$. The equation $D(ka, kL) = 0$ defines the complex resonant frequencies $\omega_{\text{res}} = ck_{\text{res}} = \omega'_{\text{res}} + i\omega''_{\text{res}}$, where c is the light velocity in vacuum. Due to the radiation loss, the quantity $\omega''_{\text{res}} = \mathrm{Im}(\omega)$ is always negative ($\omega''_{\text{res}} < 0$). Therefore, for real frequencies ($\omega'' = 0$), the denominator $D(ka, kL)$ does not vanish. But it acquires minimum values when the frequency of the incident wave is close to the real part of the resonant frequency ($\omega \approx \omega'_{\text{res}}$). This occurs when $kL \approx n\pi$ or $L \approx n\lambda/2$ with $n = 1, 2, 3, \ldots$ and results in the current resonance. Under the normal incidence (the direction of the incident wave is perpendicular to the wire axis), only the odd resonances ($n = 1, 3, 5, \ldots$) are realized due to the symmetry of the incident field [$E_z^{\text{inc}}(-z) = E_z^{\text{inc}}(z)$]. Figure 2, taken from the classic paper (11), illustrates the resonance behavior of scattering from thin wires. The incident wave direction is perpendicular to the wire axis. The quantity A in Fig. 2 is the total power of the field scattered in all directions. The maximum scattering occurs in the directions perpendicular to the wire and therefore in the backscattering direction as well. In Fig. 2, the quantity $\chi = 1/[2|\ln(k\alpha)|]$ depends on the wire radius, $2l = L$ is the wire length, and $\alpha = kl$.

A similar interference of a specular reflection with surface diffracted rays (Fig. 3) explains the backscattering from perfectly conducting spheres and prolate spheroids at the upper end of the resonance region [p. 149 of (2) and pp. 822–848 of (4)]. However, an important difference exists between the resonances in scattering from wires and spheres. The resonance backscattering from wires is caused by the current resonance in the wires and it is accompanied by a simultaneous

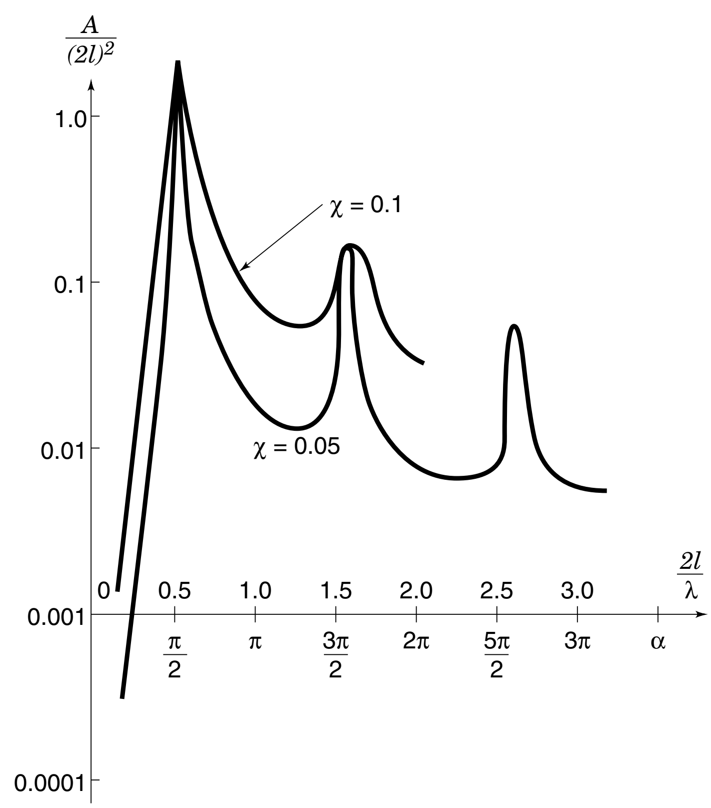

Figure 2. Integral cross section of thin wires (from Ref. 11). This quantity has the maximum (resonance) values for wires with the total length $L = 2l \approx (2n + 1)\lambda/2$, $n = 1, 2, 3, \ldots$. Along such wires from one edge to another, each multiple edge wave acquires the phase shift of $(2n + 1)\pi$. Due to reflection at the edge, it acquires an additional phase shift of π. As a result, this wave becomes equi-phased with all other multiple edge waves. This leads to the resonance behavior for the current and scattered field.

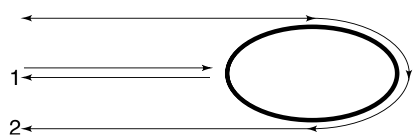

Figure 3. Backscattering from a body of revolution. The total scattered field consists of two components. One of them is a specular reflected ray (1) and the other is a beam of diffracted rays (2) radiated by creeping waves traveling along the shadow side of the scattering body. The equi-phase interference of these two components results in the resonance-like increase of the scattered field.

increase of the scattered field in other directions. This is a true resonance effect. The resonance scattering from spheres and spheroids is a simple equiphase interference in the single (backward) direction without the field increase in other directions. Additional data for the resonance backscattering can be found in (4) (pp. 822–848). As in the case of quasi-static scattering, direct numerical methods are also efficient for RCS calculations in the resonance frequency region (5–7).

QUASI-OPTICAL SCATTERING

In the quasi-optical frequency region, which is often referred to as the high-frequency region, linear dimensions of scatterers are much greater than the wavelength of the incident wave. For example, this occurs in the scattering of decimeter and centimeter radar waves by such objects as ships, airplanes, and missiles. In contrast to the quasi-static and resonance frequency regions, the scatterings by objects in the quasi-optical region are determined mainly by the objects' local properties rather than by their whole volume.

Large dimensions and complex shapes of scattering objects allow the existence of various types of scattered fields. Some of them are illustrated in Fig. 4. Geometrical optics rays and beams (A) reflected from the object provide the main contributions to backscattering. Diffraction of the incident wave at edges and at lines of curvature discontinuity or material discontinuity creates edge waves (B and C), which can be interpreted as diffracted rays. They represent the second-order contributions (12–15). Diffracted waves arising from corners provide the third-order contributions (12–14). At the shadow boundary on a smooth scattering surface, the incident wave excites creeping waves (D), which propagate along the shadow side of the object and radiate surface diffracted rays (E). Due to continuous radiation of these rays, the creeping waves attenuate exponentially and for this reason the contribution of surface diffracted rays (E) to backscattering is small (12,13). However, for the objects with dimensions comparable to the wavelength, surface diffracted rays can give appreciable contributions, as it is mentioned already in the previous section (see also Fig. 2). Diffracting waves propagating along the scattering object can undergo multiple diffractions at geometrical and material discontinuities and can transform into other types of waves. This process creates high-order contributions to backscattering (12–15). A visual description of scattering from large objects, simple quantitative estimations of some contributions to backscattering, and relevant references are presented in (16).

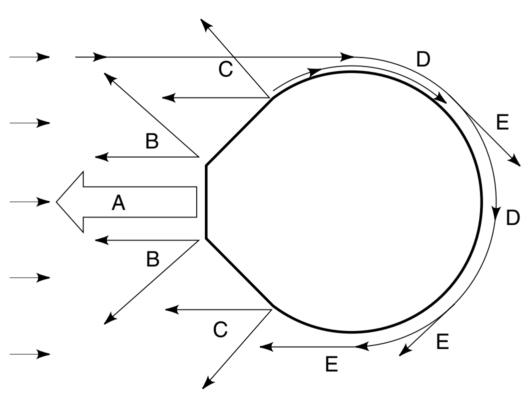

Figure 4. Backscattering from a convex opaque object. The main contributor to the scattered field is beam A reflected from the front planar facet of the object. Edge waves B are created at the edges. Edge waves C are created at the curvature discontinuities. At the shadow boundary, the incident wave excites creeping waves D which propagate along the object's surface and radiate surface diffracted rays E. Additional creeping waves are excited at the curvature discontinuities.

High-frequency asymptotic methods are widely used to predict scatterings in this frequency region. They include geometrical optics (GO) and its extension, geometrical theory of diffraction (GTD); physical optics (PO) and its extension, physical theory of diffraction (PTD); and various modifications and extensions of GTD and PTD. These asymptotic techniques are discussed in ELECTROMAGNETIC WAVE SCATTERING and RADAR CROSS-SECTIONS. The present article supplements these and concentrates mainly on the physical optics. This method is not so precise as GTD, PTD, and their extensions, but it allows useful estimations for the scattered fields in which many practical problems cannot be treated with other techniques. Direct numerical methods, in their classical forms, are not efficient in the high-frequency region. Various combinations of these methods with the asymptotic techniques (so-called hybrid methods) represent a promising direction in the prediction of high-frequency scattering (17). Additional information about numerical, hybrid, and asymptotic techniques used for the solution of scattering problems can be found in Refs. 6, 13, and 18 and in the reading list at the end of this article.

Geometrical Optics Approximation

GO is used for approximate estimations of backscattering in many practical problems. The basic notion of GO involves the concept of rays. A ray is an infinitely narrow stream of the wave field moving with the light velocity along the lines perpendicular to the phase fronts. These lines are called ray trajectories. In free space they are straight lines. Electric and magnetic vectors of the ray field are perpendicular to each other and to the direction of propagation. GO reflected rays obey simple rules (19,20): the reflected ray lies in the incidence plane which contains the incident ray and the normal to the scattering surface at the reflection point (Fig. 5); the angle of reflection equals the angle of incidence (Snell's reflection law); the power inside an elementary hypothetical tube confined by neighboring rays is constant.

GO is a good approximation for the field reflected from large smooth scattering objects. It provides the leading term in the exact high-frequency asymptotic expansion of the re-

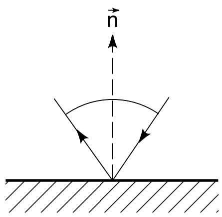

Figure 5. Reflection from a planar surface. The reflected ray lies in the plane which contains the incident ray and the unit normal vector $\boldsymbol{n}$ to the reflecting surface.

flected field. The reflection coefficient is found from the solution of an appropriate canonical problem. For opaque homogeneous objects, this is the Fresnel reflection coefficient, which determines the amplitude and phase of plane waves reflected from a planar boundary of a semi-infinite homogeneous medium [pp. 474–479 of (2)]. For opaque objects coated with thin layers, the canonical problem is the reflection of plane waves from an infinite planar layer. This canonical layer is tangential to the scattering object (Fig. 6). It is homogeneous in the directions parallel to its surface and has the same material structure in depth as a real layer at the reflection point T. The canonical layer is placed on the planar boundary of a homogeneous medium with the same material properties as a real object at the tangency point. This implies that the field on a real coated object is determined exclusively by its local properties in the vicinity of the reflection point. Nonlocal contributions from various waves propagating along the object are not treated with this approach. Creeping and traveling waves [pp. 120 and 130 of (2)] are examples of such waves.

According to this GO approach, the backscattering RCS of smooth coated objects equals

$$\sigma = |\mathbf{r}(0)|^2 \cdot \pi R_1 R_2 \qquad [(\mathrm{m})^2] \tag{10}$$

where r(0) is the reflection coefficient for the normal incidence ($\theta = 0$) and R_1, R_2 are principal radii of the curvature of the scattering surface at the reflection point T. In the case of isotropic objects and coatings, the reflection coefficient r(0) does not depend on the incident wave polarization. Equation (10) is not valid for objects with planar faces when $R_1 = R_2 = \infty$. It also fails for objects that contain ruled elements (cylindrical, conical) with a rectilinear generatrix whose radius of curvature is infinite. In this case, the rays reflected by the object form the so-called reflected beams, which undergo the transverse diffusion while propagating from the object and for this reason lose their geometrical optics structure in the far zone.

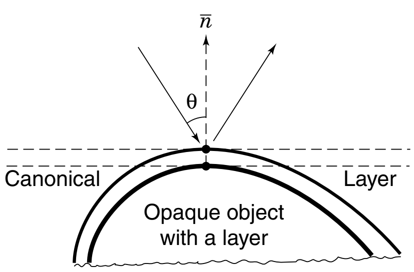

Figure 6. A scattered field at the reflection point on a coated scattering object is equal asymptotically (with $kR_{1,2} \to \infty$) to the field which would be reflected from a tangential layer with the same material properties. Due to losses, the contributions of rays and waves propagating along the object (inside the coating) become small and can be neglected.

Physical Optics Approximation

This method goes back to MacDonald (21) and is based on three concepts which are GO, canonical planar layer, and equivalency principle.

The first step in the physical optics (PO) approximation is to use GO for the description of fields right on the scattering surface where GO approximation is still valid. The second step is to calculate the scattered field outside the object using the equivalency principle described in the following. Tangential components ($\boldsymbol{n} \times \boldsymbol{E}$, $\boldsymbol{n} \times \boldsymbol{H}$) of electric and magnetic vectors of the total field on the scattering surface (with the external unit normal $\boldsymbol{n}$) can be interpreted as equivalent magnetic and electric currents

$$\begin{aligned} \boldsymbol{j}_m &= -\boldsymbol{n} \times \boldsymbol{E} \qquad (\mathrm{V/m}) \\ \boldsymbol{j}_e &= \boldsymbol{n} \times \boldsymbol{H} \qquad (\mathrm{A/m}) \end{aligned} \tag{11}$$

In the PO approach, the equivalent currents are defined in the GO approximation. The total electromagnetic field on the scattering object is considered approximately as the sum of the GO incident and reflected waves ($\boldsymbol{E}^{\mathrm{GO}} = \boldsymbol{E}^{\mathrm{inc}} + \boldsymbol{E}^{\mathrm{ref}}$, $\boldsymbol{H}^{\mathrm{GO}} = \boldsymbol{H}^{\mathrm{inc}} + \boldsymbol{H}^{\mathrm{ref}}$). Thus, the PO surface currents are defined as

$$\begin{aligned} \boldsymbol{j}_e^{\mathrm{PO}} &= \boldsymbol{n} \times \boldsymbol{H}^{\mathrm{GO}} \\ \boldsymbol{j}_m^{\mathrm{PO}} &= -\boldsymbol{n} \times \boldsymbol{E}^{\mathrm{GO}} \end{aligned} \tag{12}$$

This equation defines equivalent currents only on the illuminated side of the opaque scattering object. On the shadow side, these currents are assumed to be zero. In the particular case of perfectly conducting objects, the magnetic current does not exist ($\boldsymbol{j}_m^{\mathrm{PO}} = \mathbf{0}$) due to the boundary condition $\boldsymbol{n} \times \boldsymbol{E} = \mathbf{0}$, and the electric current equals $\boldsymbol{j}_e^{\mathrm{PO}} = 2\boldsymbol{n} \times \boldsymbol{H}^{\mathrm{inc}}$ according to the GO approximation.

The scattered field is found by the integration of equivalent currents over the scattering surface S. Geometry of a sample scattering problem is shown in Fig. 7, where the quantity r is the distance between the integration (ρ, θ, ϕ) and observation

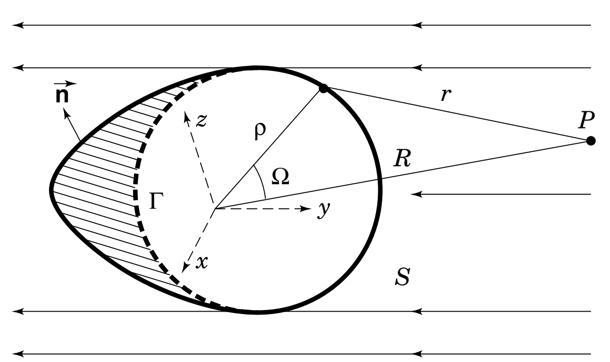

Figure 7. Schematics of a scattering problem: $\boldsymbol{S}$ is the surface of the scattering object; the dashed part of this surface (with the boundary Γ) is located in the shadow region which is hidden from the incident rays.

(R, ϑ, φ) points. In the far zone ($R > k\rho^2_{\max}$), the scattered field is determined as

$$\begin{aligned} E_\vartheta &= Z_0 H_\varphi = ik(Z_0 A^e_\vartheta + A^m_\varphi) \\ E_\varphi &= -Z_0 H_\vartheta = ik(Z_0 A^e_\varphi - A^m_\vartheta) \end{aligned} \tag{13}$$

$$\boldsymbol{A}^{e,m} = \frac{1}{4\pi}\frac{e^{ikR}}{R}\int_S \boldsymbol{j}_{e,m} e^{-ik\rho\cos\Omega}\,dS \tag{14}$$

$$\cos\Omega = \cos\vartheta\cos\theta + \sin\vartheta\sin\theta\cos(\varphi - \phi) \tag{15}$$

Here, $\boldsymbol{E}_{\varphi,\vartheta}$ is the electric field intensity (V/m); $\boldsymbol{H}_{\varphi,\theta}$ is the magnetic field intensity (A/m); $\boldsymbol{A}^e$ is the electric potential vector (A); $\boldsymbol{A}^m$ is the magnetic potential vector (V); and $Z_0 = \sqrt{\mu_0/\epsilon_0} \cong 377$ (Ω) is the impedance of vacuum.

The PO approximation for the scattered field follows from Eqs. (13) and (14) when the PO approximation given by Eq. (12) is used for equivalent surface currents and the integration region is restricted to the illuminated part of the scattering surface. The line Γ shown in Fig. 7 is the boundary between the illuminated and shadow sides of the scattering surface S. The PO approach is usually applied to large convex objects. However, it is also applicable to concave objects when the multiple GO reflections are taken into account.

Accuracy of PO. Approximate estimations for the PO scattered field [Eq. (13)] can be found by the application of asymptotic techniques to the integrals [Eq. (14)] with the PO currents [Eq. (12)]. The first term of the asymptotic expansion found in this way is correct for the fields scattered by smooth convex objects and planar plates in the specular directions predicted by GO. All higher-order terms in the PO asymptotic expansion are incorrect. Only two exceptions exist when PO provides the exact solution. The first is the scattering from the infinite perfectly conducting plane. The second is the scattering from the semi-infinite perfectly conducting paraboloid of revolution illuminated by the plane wave incident along the symmetry axis (22). In the latter case, the scattered field consists of only the GO reflected rays. Reference 22 also shows that PO provides the correct second term in the high-frequency asymptotic expansion for the specular backscattering from any convex perfectly conducting bodies of revolution when the incident wave propagates in the direction parallel to the symmetry axis.

The first term of the PO asymptotic expansion for the field scattered by smooth convex objects in specular directions represents the GO reflected rays [pp. 50–62 of (2)]. Therefore, for such objects the PO value of RCS in specular directions is asymptotically (with $k \to \infty$) equivalent to the GO estimation. However, it is well known that GO is valid only away from the forward direction, i.e., from the shadow boundary of the incident rays. But PO is more general than GO and is applicable in the vicinity of this direction. All known results show that the first term of the PO asymptotic expansion for the field scattered in the forward direction is correct and leads to the following RCS for large opaque objects:

$$\sigma = 4\pi\frac{A^2}{\lambda^2} \qquad [(\mathrm{m})^2] \tag{16}$$

Here, the quantity A is the area of the scattering object projection on the plane perpendicular to the direction of the incident wave propagation.

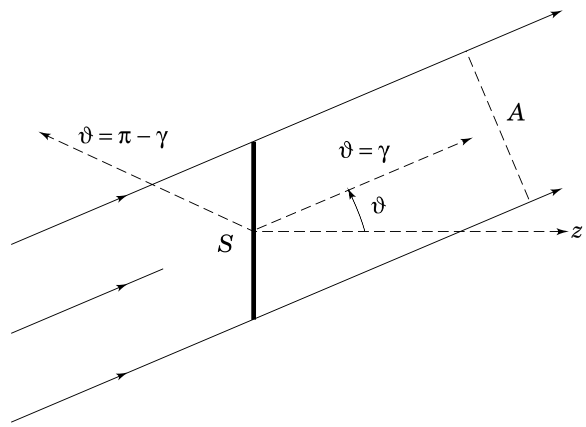

Figure 8. Directions of the forward ($\vartheta = \gamma$) and specular ($\vartheta = \pi - \gamma$) scattering from the plate $\boldsymbol{S}$. The dashed line $\boldsymbol{A}$ denotes the projection of the plate $\boldsymbol{S}$.

Reference 23 contains similar PO estimations for thin semi-transparent plates. The field on the plate surface is defined by complex reflection and transmission coefficients which depend on the incidence angle (γ) and polarization of the incident wave. The incident wave with an arbitrary linear polarization can be decomposed into two independent waves with orthogonal polarizations. A decomposition is chosen such that either the electric or magnetic vector of the incident wave is parallel to the plate. In the first case, denote the reflection and transmission coefficients for the electric vector as $r_e(\gamma)$ and $t_e(\gamma)$, respectively. Similar coefficients, $r_h(\gamma)$ and $t_h(\gamma)$, for the magnetic vector describe the plate when the magnetic vector of the incident wave is parallel to the plate. Reference 2 (pp. 479–499) contains instructions for the calculation of these coefficients. Two directions of scattering are of greatest interest. The first is the direction of specular reflection, $\vartheta = \pi - \gamma$, and the second is the forward direction, $\vartheta = \gamma$ (Fig. 8). According to (23), the PO approximations of RCS in the specular direction are given by

$$\begin{aligned} \sigma_e(\pi - \gamma) &= 4\pi\frac{A^2}{\lambda^2}|r_e(\gamma)|^2 \\ \sigma_h(\pi - \gamma) &= 4\pi\frac{A^2}{\lambda^2}|r_h(\gamma)|^2 \end{aligned} \tag{17}$$

and in the forward direction by

$$\begin{aligned} \sigma_e(\gamma) &= 4\pi\frac{A^2}{\lambda^2}|1 - t_e(\gamma)|^2 \\ \sigma_h(\gamma) &= 4\pi\frac{A^2}{\lambda^2}|1 - t_h(\gamma)|^2 \end{aligned} \tag{18}$$

where the quantity A is the same as in Eq. (16). This is the area of the plate projected on the plane perpendicular to the direction of the incident wave. Equations (17) and (18) are applicable for planar plates of an arbitrary shape under the condition $A \gg \lambda^2$. This means that the grazing angles ($\gamma \approx \pi/2$) cannot be treated with these equations.

Known results for perfectly conducting plates ($|r_{e,h}(\gamma)| = 1$, $|t_{e,h}(\gamma)| = 0$) show that PO estimations given in Eqs. (17) and (18) are correct. These equations also give the correct result, $\sigma_h(\pi/2) = 0$, for perfectly conducting plates under the grazing

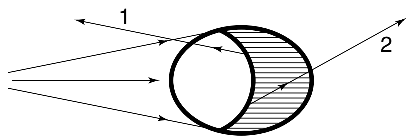

Figure 9. The PO current given by Eq. (12) is discontinuous at the shadow boundary of the scattering surface. This leads to spurious waves (1 and 2) in the case of a smooth scattering surface.

incidence. In this case, the incident wave does not undergo diffraction because its electric vector is perpendicular to the plate surface. PO describes satisfactorily the field scattered from large conducting plates not only in the specular and forward directions corresponding to main lobes in the directivity pattern, but also in the directions of neighboring side lobes. However, PO fails to predict a field level in minimums of the directivity pattern [Figs. 7-19 and 7-20 on p. 509 of (2)] and does not satisfy the reciprocity principle.

The PO currents given by Eq. (12) are discontinuous on the shadow boundary of a scattering surface. The PO field contains spurious waves from such a boundary in the case of smooth scattering surfaces (Fig. 9). A similar current discontinuity on scattering objects with edges results in edge waves. If the scattering edge is visible from the observation point, such an edge wave does exist. The PO edge waves coming from invisible edges are spurious shooting-through waves (Fig. 10). Such shooting-through waves do not occur in the backscattering direction. All PO spurious waves can be removed by neglecting the corresponding terms in the asymptotic expansion of the integral in Eq. (14). For real edge waves, even the first-order term of their PO asymptotic expansion is incorrect. This defect is remedied in PTD by the inclusion of the field radiated by the so-called nonuniform currents arising from the diffraction of the incident wave at edges (14,15).

One should emphasize a special role of PO in PTD. PO is a constitutive part of PTD. Therefore, the PO's first- and higher-order asymptotic terms are integral parts of the PTD asymptotic expansions for the total scattered field. For example, the terms with coefficients $(3d/16a)$ in the PTD equations (99) and (100) of (15) are exactly the PO's second-order terms in the asymptotic expansion of the field scattered by a perfectly conducting cylinder of finite length.

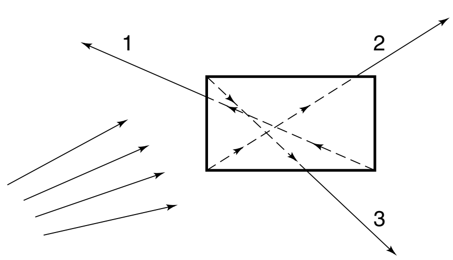

Figure 10. A scattered field is generated by the induced surface currents. Any approximations for these currents can result in the appearance of nonphysical components in the scattered field. In particular, the PO currents create spurious shooting-through edge waves (1, 2, and 3) passing through an opaque object.

Polarization of the PO Scattered Field. In general cases, components E_ϑ and E_φ in Eq. (13) have different amplitudes and phases. This results in the elliptic polarization of the scattered field even in the case when the incident wave is linearly polarized. This means that the electric vector of the scattered field rotates with the angular frequency $\omega = k \cdot c$ and its endpoint traces an ellipse. The direction of rotation (clockwise or counterclockwise) is determined by the phase shift between components E_ϑ and E_φ. The lengths of the elliptical axes are determined by the amplitudes of these components. Due to diffraction, the scattered field can contain an electric field component perpendicular to the incident wave polarization. This phenomenon is known as *depolarization,* or *crosspolarization.*

The PO field scattered by arbitrary perfectly conducting objects in the backscattering direction does not contain the crosspolarized component [p. 56 of (2)]. It is assumed only that no multiple GO reflections occur on the objects' surface. This PO result is correct for scattering objects with certain symmetry. These are objects with a symmetry plane parallel both to the electric (or magnetic) vector of the incident wave and to the direction of its propagation. Each element of such a scattering object may create the crosspolarized component. But due to the symmetry, the crosspolarized components from symmetrical elements cancel each other in the backscattering direction (Fig. 11). A convex smooth body of revolution whose symmetry axis is parallel to the incident wave direction is a simple example of such an object. A symmetrical plate, illuminated by the plane wave whose electric (or magnetic) vector and direction of propagation are parallel to the symmetry plane, is another example where the backscattered field does not contain a crosspolarized component (Fig. 12).

As previously stated, the first term of the PO high-frequency asymptotic expansion represents the GO reflected ray. This ray contains the crosspolarized component when the electric vector of the incident ray makes any angle different from 0° and 90° with the incidence plane at the reflection point. This is the case when PO correctly describes depolarization of the scattered field in the high-frequency asymptotic limit ($k \to \infty$). However, PO fails to predict all depolarization effects caused by the diffraction part of equivalent surface currents.

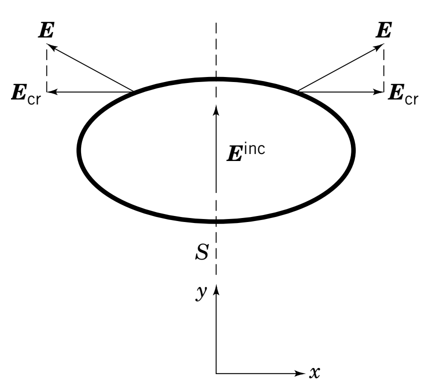

Figure 11. Backscattering without depolarization from a symmetrical perfectly conducting surface $\boldsymbol{S}$. The incident wave direction is parallel to the symmetry plane $\boldsymbol{y}$-$\boldsymbol{z}$. Vectors $\boldsymbol{E}_{cr}$ are the cross-polarized components of the reflected field. Due to the symmetry, they cancel each other.

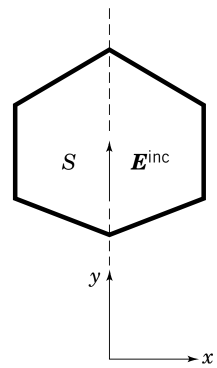

Figure 12. Backscattering without depolarization from a perfectly conducting plate $\boldsymbol{S}$. The incident wave direction is parallel to the symmetry plane $\boldsymbol{y}$-$\boldsymbol{z}$. Cross-polarized components scattered by the left and right parts of the plate are symmetrical and completely cancel each other.

Bistatic RCS. Bistatic RCS determines the power flux density of electromagnetic waves scattered by the object in an arbitrary direction. The angle between the directions to the transmitter and receiver is called the bistatic angle. Monostatic, or backscattering, RCS is a particular case of bistatic RCS when the bistatic angle equals zero. Some PO results for bistatic RCS have already been discussed. This section addresses the interrelationships between bistatic and monostatic RCS.

Using PO, one can prove the following statement:

> For perfectly conducting bodies which are sufficiently smooth, in the limit of vanishing wavelength, the bistatic cross section is equal to the monostatic cross section at the bisector of the bistatic angle between the direction to the transmitter and receiver.
>
> *[pp. 157–160 of (1) and p. 11 of (2)]*

There is a simple physical explanation for this result. As already stated, the first term of the PO asymptotic expansion for the field scattered by smooth objects exactly equals the GO expression for the reflected rays. The monostatic RCS caused by these rays is given by Eq. (10). In the case of perfectly conducting objects, this equation reduces to

$$\sigma = \pi R_1 R_2 \tag{19}$$

It should be noted that this equation is valid also for the bistatic RCS, which therefore *does not depend on the bistatic angle* $\beta = 2\vartheta$ (Figs. 5 and 6). This follows directly from Eqs. (5.32), (6.19), and (6.20), given in Chapter 8 of (19):

$$\begin{aligned} \boldsymbol{E}(r) &= \frac{1}{2}\boldsymbol{E}(0)\sqrt{R_1R_2}\,\frac{e^{iks}}{s} \\ \boldsymbol{H}(r) &= \frac{1}{2}\boldsymbol{H}(0)\sqrt{R_1R_2}\,\frac{e^{iks}}{s} \end{aligned} \tag{20}$$

These expressions describe the field reflected by smooth convex objects at a far distance ($s \gg R_{1,2}$) from the reflection point for *any incidence angle* ($0 \le \vartheta < \pi/2$). In the case of reflection from concave surfaces, the reflected field acquires the additional phase shift of ($-\pi/2$) in passing through a focus of reflected rays. Vectors $\boldsymbol{E}(0)$ and $\boldsymbol{H}(0)$ denote the reflected field at the reflection point. Expressions (20) clearly show that the GO reflected field really does not depend on the incidence angle. As a result, the bistatic RCS does not depend on the bistatic angle and is the same as the monostatic RCS at the bisector direction that is perpendicular to the scattering surface at the reflection point. Thus, the cited equivalence between the bistatic and monostatic RCS is a pure GO effect and is fulfilled asymptotically (with $k \to \infty$) only in the ray region, away from the shadow boundary behind the scattering object. It is also clear that this equivalence is not applicable when the scattered field contains multiple reflected rays arising from concave parts of the scattering surface. Reference 1 (pp. 160–183) presents additional results for bistatic RCS of some typical objects found using PO and other approximations.

In the case of coated smooth objects, Eq. (20) leads to the bistatic RCS

$$\sigma(\vartheta) = |\mathrm{r}_{e,h}(\vartheta)|^2 \pi R_1 R_2 \tag{21}$$

where the reflection coefficients $\mathrm{r}_{e,h}(\vartheta)$ depend on the polarization and direction of the incident wave. Therefore, the asymptotic equivalence between bistatic and monostatic RCS can be valid only for those bistatic angles where $|\mathrm{r}_{e,h}(\vartheta)| = |\mathrm{r}_{e,h}(0)|$.

This discussion relates to the situation where the bistatic scattered field is produced by a single scattering source (the reflection point). The field scattered by complex objects can have many sources (scattering centers) on the object's surface. Figure 13 illustrates the bistatic scattering from the center located at the point (x_n, y_n, z_n). The origin of Cartesian coordinates is somewhere inside the scattering object. The z-axis is directed along the bisector of the bistatic angle β. In the far zone, the bistatic scattered field can be represented as the sum of partial contributions from all scattering centers [pp. 983–988 of (4)]:

$$\boldsymbol{u}(\beta) = \frac{e^{ikR}}{R}\sum_n \boldsymbol{v}_n e^{-2ikz_n\cos\frac{\beta}{2}} \tag{22}$$

Here, $\boldsymbol{u}$ is either the electric or magnetic vector of the total scattered field; R is the distance from the origin to the observation point. Vector $\boldsymbol{v}_n$ determines the amplitude and polarization of the wave generated by the nth scattering center. Suppose that vectors $\boldsymbol{v}_n$ and the number of scattering centers are constant inside the angular sector $0 \le \beta \le \beta_{\max}$. Assume also that coordinates z_n of scattering centers do not depend on the bistatic angle β, while coordinates x_n and y_n can be func-

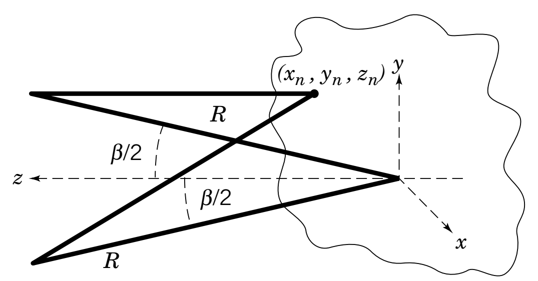

Figure 13. Geometry of the bistatic scattering problem. A solid winding line represents a scattering object with many scattering centers ($\boldsymbol{x_n}$, $\boldsymbol{y_n}$, $\boldsymbol{z_n}$). The scattering direction forms the angle β with the direction of the incident wave.

tions of this angle. Under these conditions, the monostatic field scattered in the bisector direction equals

$$\boldsymbol{u}(0) = \frac{e^{ikR}}{R}\sum_{n}\boldsymbol{v}_n e^{-2ikz_n} \tag{23}$$

Comparisons of Eqs. (22) and (23) show that the bistatic RCS, $\sigma(\beta, k)$, at the frequency $\omega = c \cdot k$ will be equal to the monostatic RCS, $\sigma[0, k\cos(\beta/2)]$, at the frequency $\omega = c \cdot k \cdot \cos(\beta/2)$. This equality requires the additional assumption that each vector $\boldsymbol{v}_n$ is constant in the frequency band $[c \cdot k\cos(\beta/2) \leq \omega \leq c \cdot k]$. The derivation, some applications, and restrictions of this equivalence relation are presented in (4) (pp. 983–988). In particular, this reference notes that this equivalence is not true for the bistatic scattering from spheres when the bistatic angle exceeds one degree and the sphere radius is less than 6λ. Before applying this equivalence in practice, we must first check carefully that all assumptions made in this scattering model are really fulfilled. One can expect that this approximate model can be reasonable only for small bistatic angles.

PTD as an Extension of PO. PTD is a natural extension of PO (14,15,24). In PTD, the PO current given by Eq. (12) is considered as the uniform component (j^0) of the total surface current and is supplemented by the additional, nonuniform component (j^1). In contrast to the PO current that has the GO origin, the nonuniform current is caused by diffraction at smooth bendings, sharp edges, corners, and any other geometrical discontinuity and material inhomogeneity on the scattering surfaces. Creeping and edge current waves are examples of such a current. The field generated by the nonuniform current represents the PTD contribution to the scattered field. Exact analytical expressions for nonuniform currents are not available. Therefore, one has to find their high-frequency approximations by the solution of appropriate canonical problems. In this manner, Fock developed special functions which describe the nonuniform current on smooth convex objects in the vicinity of the shadow boundary (19). The Sommerfeld solution of the wedge canonical problem is used for the asymptotic description of the nonuniform current near perfectly conducting edges (14,15,24). The concept of uniform and nonuniform currents plays a key role in PTD and those hybrid techniques that combine direct numerical methods with high-frequency asymptotic approximations (6,17,18). Reference 15 shows that PTD properly defines the leading term in the high-frequency asymptotic expansions for primary and multiple edge waves. A close connection exists between PTD and GTD. The latter automatically follows from the PTD integrals when they are evaluated by the stationary phase technique [pp. 136–138 of (15)]. Some PTD results are presented in the next section.

BACKSCATTERING RCS OF SIMPLE SHAPES

This section contains examples of PO estimations for RCS of simple objects. Whenever possible, these estimations are accompanied by more precise PTD counterparts that include the contributions of primary edge waves generated by the nonuniform edge currents. Only objects with symmetry of revolution are considered. All given data are taken from (15) and (16). Exact, numerical solutions of scattering problems for bodies of revolution can be found, for example, in (6), (18), and (25).

Semitransparent Disk

The geometry of this scattering problem is shown in Fig. 8. The backscattering direction is determined by the spherical coordinates $\vartheta = \pi - \gamma$, $\varphi = -\pi/2$. The disk radius is denoted by the letter a. The incident wave can have either E- or H-polarization. In the first case, the electric vector is perpendicular to the incidence plane and parallel to the disk face. The disk properties are described by the reflection and transmission coefficients, $r_e(\gamma)$, $t_e(\gamma)$, with respect to the electric vector. In the case of H-polarization, the magnetic vector of the incident wave is perpendicular to the incident plane and parallel to the disk face. The reflection and transmission coefficients, $r_h(\gamma)$, $t_h(\gamma)$, determine the magnetic vector on the front ($z = -0$) and rear ($z = +0$) faces of the disk, respectively. According to Eq. (67) in (23), the backscattering RCS is given by

$$\begin{aligned}\sigma_e^{\text{PO}}(\gamma) &= |r_e(\gamma)|^2\pi a^2[J_1(2ka\sin\gamma)]^2\cot^2\gamma \\ \sigma_h^{\text{PO}}(\gamma) &= |r_h(\gamma)|^2\pi a^2[J_1(2ka\sin\gamma)]^2\cot^2\gamma\end{aligned} \tag{24}$$

where $J_1(x)$ is the Bessel function and the incidence angle is restricted by the values $0 \leq \gamma < \pi/2$. For perfectly conducting disks, one should put $r_e(\gamma) = -1$ and $r_h(\gamma) = +1$. Then, in the case of the normal incidence ($\gamma = 0$), Eq. (24) reduces to

$$\sigma_e^{\text{PO}} = \sigma_h^{\text{PO}} = \pi a^2(ka)^2 \tag{25}$$

Figure 7-24 on p. 514 of (2) shows that this equation is in good agreement with the exact results when $ka \geq 5$. Note also that Eq. (18), with $A = \pi a^2\cos\gamma$, determines the PO bistatic RCS of this disk for the forward direction ($\vartheta = \gamma$). PTD estimations for RCS of a perfectly conducting disk are presented in Chapters 2 and 5 of (14). See also pp. 514–521 of (2). Some important corrections in the PTD expressions for bistatic scattering from a disk are given in (24). Contributions of multiple edge waves to forward scattering are presented in (15) (pp. 149–151).

Circular Cone

Geometrical parameters of a perfectly conducting cone are shown in Fig. 14. The incident wave direction is parallel to the symmetry axis of the cone. The PO backscattering RCS is

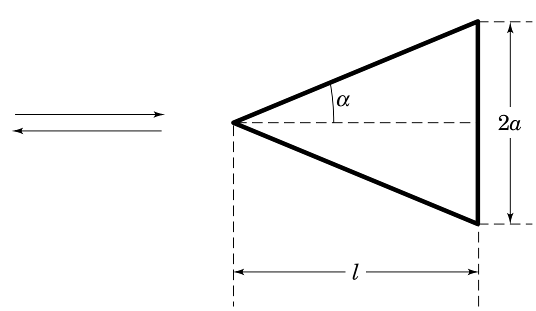

Figure 14. Backscattering from a truncated cone. The base diameter of the cone ($2a$) is large compared to the wavelength. The length of the cone (l) can be arbitrary. In the limiting case $l = 0$, the cone transforms into a disk.

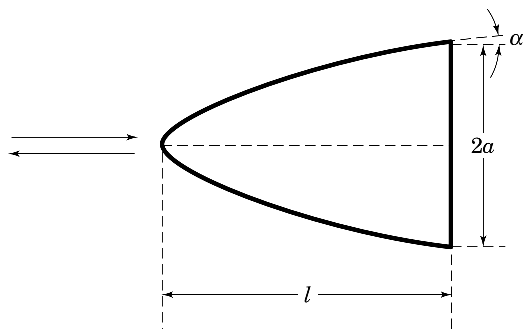

Figure 15. Backscattering from a truncated paraboloid. The base diameter of the paraboloid ($2a$) is large compared to the wavelength. The length of the paraboloid (l) can be arbitrary. In the limiting case $l = 0$, the paraboloid transforms into a disk.

given by Eqs. (17.06) and (17.09) in (15),

$$\sigma^{\mathrm{PO}} = \pi a^2 \cdot \left| \frac{1}{ka} \tan^2 \alpha \sin kl - \tan \alpha e^{ikl} \right|^2 \tag{26}$$

where the cone length equals $l = a \cot \alpha$. To clarify the physics in this equation, we rewrite it as

$$\sigma^{\mathrm{PO}} = \pi a^2 \left| \frac{i}{2ka} \tan \alpha e^{-ikl} - \left(\tan \alpha + \frac{i}{2ka} \tan \alpha \right) e^{ikl} \right|^2 \tag{27}$$

The first term (with exponential e^{-ikl}) is related to the wave scattered by the cone tip. Comparison with the exact solution [Fig. 18.15 on p. 691 of (3)] shows that this PO approximation is quite satisfactory for all cone angles ($0 \leq \alpha \leq \pi/2$). The second term (with the exponential e^{ikl}) describes the edge wave contribution. This PO approximation is incorrect. PTD takes into account the additional contribution from the nonuniform (diffraction) currents located near the cone edge and provides a more accurate result, given by Eqs. (17.06) and (17.08) in (14),

$$\sigma^{\mathrm{PTD}} = \pi a^2 \cdot \left| \frac{1}{ka} \tan^2 \alpha \sin kl + \frac{\frac{2}{n} \sin \frac{\pi}{n}}{\cos \frac{\pi}{n} - \cos \frac{2\alpha}{n}} e^{ikl} \right|^2 \tag{28}$$

where $n = 3/2 + \alpha/\pi$. When the cone transforms into the disk ($\alpha \to \pi/2$, $l \to 0$) the previous expressions reduce to

$$\sigma^{\mathrm{PO}} = \sigma^{\mathrm{PTD}} = \pi a^2 (ka)^2 \tag{29}$$

which coincides with Eq. (25).

Paraboloid

The directrix of a paraboloid is given by the equation $r = 2pz$ where $p = a \tan \alpha$ (Fig. 15). The length of the paraboloid equals $l = a^2/(2p) = (a/2)\cot \alpha$. The angle α is formed by the symmetry axis z and the tangent to the directrix at the point $z = l$. The radius of the paraboloid base equals a. The incident wave propagates in the positive direction of the z-axis. According to Eq. (18.02) in (14), the PO backscattering RCS of a perfectly conducting paraboloid equals

$$\sigma^{\mathrm{PO}} = 4\pi a^2 \tan^2 \alpha \sin^2 kl \tag{30}$$

This equation can be written in another form as

$$\sigma^{\mathrm{PO}} = \pi a^2 \tan^2 \alpha \cdot |e^{-ikl} - e^{ikl}|^2 \tag{31}$$

which is more convenient for the physical analysis. The term with the exponential e^{-ikl} gives the correct contribution of the specular reflection from the paraboloid tip. The term with the exponential e^{ikl} represents the edge wave contribution and is wrong. PTD includes the additional contribution from the nonuniform edge currents and provides the correct result, given by Eq. (18.04) in (14):

$$\sigma^{\mathrm{PTD}} = \pi a^2 \left| \tan \alpha + \frac{\frac{2}{n} \sin \frac{\pi}{n}}{\cos \frac{\pi}{n} - \cos \frac{2\alpha}{n}} e^{2ikl} \right|^2 \tag{32}$$

where $n = 3/2 + \alpha/\pi$. When the paraboloid transforms into the disk ($\alpha \to \pi/2$ and $l \to 0$), these expressions reduce to Eq. (29).

Truncated Sphere

The geometry of this scattering problem is shown in Fig. 16. The angle α is formed by the tangent to the sphere generatrix and the symmetry axis. The sphere radius equals $\rho = a/\cos \alpha$, where a is the base radius. The length of the truncated sphere equals $l = \rho \cdot (1 - \sin \alpha)$. It is assumed that $l \leq \rho$. The PO backscattering RCS of a perfectly conducting sphere equals [Eq. (19.05) in (14)]

$$\sigma^{\mathrm{PO}} = \pi a^2 \left| \frac{1}{\cos \alpha} - \frac{i}{2ka} - \left(\tan \alpha - \frac{i}{2ka} \right) e^{2ikl} \right|^2 \tag{33}$$

In this equation, the first two terms represent the specular reflection from the sphere, and both are correct. The third term (with the exponential e^{2ikl}) gives the contribution from the edge and it is wrong. With $ka \gg 1$, Eq. (33) simplifies to

$$\sigma^{\mathrm{PO}} = \pi a^2 \left| \frac{1}{\cos \alpha} - \tan \alpha e^{2ikl} \right|^2 \tag{34}$$

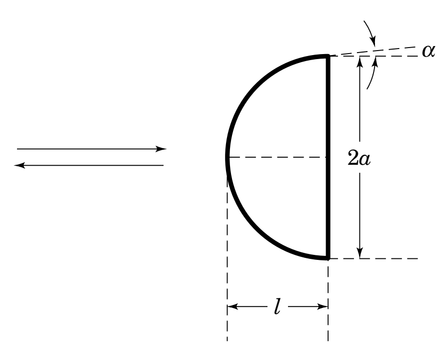

Figure 16. Backscattering from a truncated sphere. The base diameter of the sphere ($2a$) is large compared to the wavelength. The length of the sphere (l) can be arbitrary. In the limiting case $l = 0$, the sphere transforms into a disk.

When $\alpha = 0$, the latter gives the RCS of a hemisphere, $\sigma = \pi a^2$. The PTD backscattering RCS is determined by Eq. (19.12) in (14),

$$\sigma^{\mathrm{PTD}} = \pi a^2 \left| \frac{1}{\cos\alpha} + \frac{\frac{2}{n}\sin\frac{\pi}{n}}{\cos\frac{\pi}{n} - \cos\frac{2\alpha}{n}} e^{2ikl} \right|^2 \qquad (35)$$

where $n = 3/2 + \alpha/\pi$. When the sphere transforms into the disk ($\alpha \to \pi/2$, $\rho \to \infty$, $l \to 0$), Eqs. (34) and (35) reduce exactly to Eq. (29).

Circular Cylinder with Flat Ends

The diameter and length of a perfectly conducting cylinder are assumed to be large as compared with the wavelength of the incident wave. PO and PTD estimations for backscattering RCS are developed in Chapter 3 of (14). They are also presented in (2) (pp. 308–312). PTD asymptotic expressions for bistatic RCS are given in (15) (pp. 152–154).

BACKSCATTERING FROM COMPLEX OBJECTS AND STEALTH PROBLEMS

Computer codes based on GTD, PTD, and on their hybridizations have been developed for prediction of high-frequency scattering from complex perfectly conducting objects. Relevant references can be found in (16), (18), and in special issues of *Proc. IEEE* (1989), *IEEE Trans. Antennas Propag.* (1989), and *Annales des Telecommunications* (1995), which are mentioned in the reading list. Note also the XPATCH code (based on the shooting-and-bouncing ray technique and PTD), which allows the calculation of backscattering from complex geometries. Information about this code is published in *IEEE Trans. Anntennas Propagat. Magazine,* **36** (1), pp. 65–69, 1994. Computer codes interfaced with graphical utilities of workstations can display three-dimensional chromatic views of scattering centers and magnitudes of their contributions to RCS. This is the end result of complicated computations. However, a part of this can be obtained without any computations. Nature can show us the location of all scattering centers if we bring a small metallized model of the scattering object into an anechoic optical chamber and illuminate the model by the light. Bright shining points (scattering centers) seen on a scattering object are exactly those from which the radar waves will be reflected toward the radar, if we look at the object from the light source direction. (The following text is taken from Ref. 16 and slightly modified.)

The locations of these points do not depend on the frequency of incident electromagnetic waves, and they are determined completely by the location of the light source (the radar), the observer, and the scattering object. These shining points obey the Fermat principle. This means that the path along the ray between the source, the reflecting point, and the observer is extremal (minimal or maximal) in comparison with similar paths corresponding to neighboring points on the object's surface. A more detailed description of the Fermat principle is presented for example in Section 3.3.2 in Ref. 20.

Waves reflected from discrete shining points located on the smooth parts of the scattering object represent the usual geometrical optics reflected rays. Waves reflected from discrete shining points located on edges, tips, and corners are diffracted rays. The farthest shining points on a smooth object, i.e., those located on the boundary between visible and invisible sides of the object, create surface diffracted rays.

As the orientation of the object is changed, the shining points move along the object. Some of them can merge with each other and create a brighter point. In this case our eyes (i.e., the radar) are located on a caustic is the envelope of merged rays.

We can also observe bright shining lines and bright shining spots on the object, which contain an *infinite* number of continuously distributed shining points. The important property is that the optical path through a shining point from the source to the observer is constant for all of these points. It is assumed here that the source and observer are far from the scattering object. All reflected waves from these points reach the observer with the same phase. From the mathematical point of view, each such point is a stationary point of the infinite order: the derivatives (of any higher order) of the wave phase along the shining line (or along the shining spots) are zero at these points.

Shining spots and lines located on smooth parts of the scattering surface generate powerful reflected beams (such as those radiated by reflector antennas) which represent the strongest contributors to RCS. Shining edge lines create edge-diffracted beams whose contributions can be comparable with those from ordinary reflected rays.

It is difficult to model in optics the electromagnetic properties of realistic scattering surfaces for the radar frequency band. But the optical modeling can be used to identify the scattering centers and to control them by an appropriate shaping of the scattering surface. As it is well known, one of the basic ideas of the current stealth technology is to use an appropriate body shaping and to shift all reflected beams and rays away from the directions to the radar. See, for example, Refs. 2, 16, and the radar cross-section handbooks mentioned in the reading list. Some interesting details about the development of stealth technology in the United States are presented in Refs. 26–28.

The second idea of stealth technology is traditional: to use radar absorbing materials (RAMs) and composite structures in order to reduce the intensity of reflected beams and rays. References 2, 16, 29, and radar handbooks (mentioned in the reading list) describe fundamental concepts used in the design and application of RAMs. We present here some details taken from Ref. 16. In order to use RAMs efficiently, it is necessary to place an electric (magnetic) RAM in the region where the average electric (magnetic) field is maximal. Location of these regions in the vicinity of real objects depends on many factors, such as the radar frequency, geometry, size, and electrical properties of the object, as well as properties of materials intended for absorption. Identification of such regions and optimization of the RAM parameters to minimize RCS is a very complex problem. Its solution is attainable only in some simple cases. Most of these relate to absorbing layers on an infinite metallic plane. From the physical point of view such absorbing layers can be considered as open resonators that can support eigen-oscillations. Frequencies of eigen-oscillations are complex quantities. Their imaginary part is responsible for the loss inside the resonator and radiation from the resonator. It turns out that the minimal reflection from such resonators happens when the frequency of an incident wave is close to the real part of the resonator eigenfrequency.

Note that thin electric RAMs are not efficient when applied on metallic objects. This is due to the boundary condition: the tangential component of the electric field is very small on the metal surface. On the contrary, magnetic absorbing materials can be applied directly to the surface of a metallic object. This is an important advantage of magnetic materials over electric ones.

However, any RAMs (electric, magnetic, and hybrid) homogeneous in the direction parallel to the reflecting plate are not efficient for grazing incidence ($\theta \approx 90°$, in Fig. 5). In this case, the reflection coefficient tends to unity independently of the incident wave polarization when $\theta \rightarrow 90°$. This is a fundamental limitation of ordinary RAMs. They do not work against grazing incident waves. That is why ordinary RAMs do not reduce forward scattering. Actually, the RAM terminology is justified only for incidence angles that are not too far from $\theta = 0$ and when the reflection coefficient is small enough.

Various geometrical and material inhomogeneities on the scattering surface can partially transform the incident wave into surface waves propagating along absorbing layers. This may be used to further reduce the RCS. However, this idea has two essential defects. First, any inhomogeneity creates an additional undesirable scattered field. Second, it is not a simple problem to design an absorbing layer that would allow the propagation of surface waves. To support surface waves with the electric vector parallel to the incidence plane, the surface impedance must be inductive. But the surface impedance must be capacitive to support surface waves with the electric vector perpendicular to the incidence plane. This means that the surface impedance, and therefore the absorbing layer, must depend on the radar polarization with respect to the incidence plane. But this plane is different at different points of the scattering surface and different at the same point when the scattering object changes its orientation with respect to radar. It is very difficult and probably impossible to design such an absorber, especially against radars with circular polarization. However, for some chosen orientations of the object and for an appropriate polarization of the incident wave, this might not be a hopeless problem.

Development of efficient hybrid techniques and computer codes to predict RCS of large complex objects with realistic materials and research efforts to overcome the above physical limitations in RCS reduction represent challenging problems for future stealth technology. One can expect that future advanced computer codes will contain as necessary constitutive components the known high-frequency techniques (such as GTD, PTD, and the Uniform Theory of Diffraction) extended for coated and composite objects. Diffraction coefficients used in these techniques can be determined by the numerical solution of appropriate canonical problems. Direct numerical methods should be used for calculation of scattering from those elements of the scattering object that cannot be treated by high-frequency methods. Diffraction interaction between the object's elements handled by high-frequency techniques and by direct numerical methods can be described by the surface integral equations.

BIBLIOGRAPHY

1. J. W. Crispin Jr. and K. M. Siegel (eds.), *Methods of Radar Cross-Section Analysis.* New York: Academic Press, 1968.
2. G. T. Ruck, D. E. Barrick, W. D. Stuart, and C. K. Kirchbaum, *Radar Cross-Section Handbook,* Vol. 1 and 2. New York: Plenum Press, 1970.
3. J. J. Bowman, T. B. A. Senior, and P. L. E. Uslenghi (eds.), *Electromagnetic and Acoustic Scattering by Simple Shapes.* New York: Hemisphere Publishing Corp., 1987
4. P. C. Fritch (ed.), *Special Issue on Radar Reflectivity, Proc. IEEE,* **53** (8): August 1965.
5. M. N. O. Sadiku, *Numerical Techniques in Electromagnetics.* Boca Raton, FL: CRC Press, 1992.
6. E. K. Miller, L. Medgyesi-Mitschang, and E. H. Newman, *Computational Electromagnetics,* New York: IEEE Press, 1991.
7. P. P. Silvester and G. Pelosi (eds.), *Finite Elements for Wave Electromagnetics,* New York: IEEE Press, 1994.
8. P. Ya. Ufimtsev and A. P. Krasnozhen, Scattering from a straight thin wire resonator, *Electromagnetics,* **12** (2): 133–146, 1992.
9. L. A. Vainshtein, Waves of current in a thin cylindrical conductor, II. The current in a passive oscillator, and the radiation of a transmitting antenna, *Sov. Phys., Tech. Phys.,* **4** (6): 617–626, December 1959.
10. L. A. Vainshtein, Waves of current in a thin cylindrical conductor, III. Variational method and its application to the theory of ideal and impedance conductors, *Sov. Phys., Tech. Phys.,* **6** (1): 19–29, July 1961.
11. M. A. Leontovich and M. L. Levin, Towards a theory on the simulation of oscillations in dipole antennas, *Zhurnal Technicheskoi Fiziki,* **14** (9): 481–506, 1944 (in Russian). [The English translation is published in the report: K. C. Chen (ed.), SAND91-0720, UC-705, Sandia National Laboratories, Albuquerque, NM and Livermore, CA, Contract DE-AC04-76DP00789, January 1992].
12. J. B. Keller, Geometrical theory of diffraction, *J. Opt. Soc. Am.,* **52**: 116–130, 1962.
13. R. C. Hansen (ed.), *Geometrical Theory of Diffraction,* New York: IEEE Press, 1981.
14. P. Ya. Ufimtsev, *Method of Edge Waves in the Physical Theory of Diffraction.* Moscow: Soviet Radio Publishing House, pp. 1–243, 1962. Translated by U.S. Air Force, Foreign Technology Division, Wright-Patterson AFB, Ohio, 1971; Technical Report AD No. 733203, DTIC, Cameron Station, Alexandria, VA.
15. P. Ya. Ufimtsev, Elementary edge waves and the physical theory of diffraction, *Electromagnetics,* **11** (2): 125–160, 1991.
16. P. Ya. Ufimtsev, Comments on diffraction principles and limitations of RCS reduction techniques, *Proc. IEEE,* **84** (12): 1830–1851, 1996.
17. D. P. Bouche, F. A. Molinet, and R. Mittra, Asymptotic and hybrid techniques for electromagnetic scattering, *Proc. IEEE,* **81**: 1658–1684, 1993.
18. W. R. Stone (ed.), *Radar Cross Section of Complex Objects,* New York: IEEE Press, 1990.
19. V. A. Fock, *Electromagnetic Diffraction and Propagation Problems.* London: Pergamon Press, 1965.
20. M. Born and E. Wolf, *Principles of Optics,* New York: Pergamon, 1975.
21. H. M. Macdonald, The effect produced by an obstacle on a train of electric waves, *Phil. Trans. Roy. Soc. Lond., Series A, Math. Phys. Sci.,* **212**: 299–337, 1912.
22. C. E. Schensted, Electromagnetic and acoustic scattering by a semi-infinite body of revolution, *J. Appl. Phys.,* **26**: 306–308, 1955.

23. P. Ya. Ufimtsev, Diffraction of electromagnetic waves at blackbodies and semi-transparent plates, *Radiophys. Quantum Electr.,* **11**: 527–538, 1968.
24. P. Ya. Ufimtsev, Comments on "Comparison of three high frequency diffraction techniques," *Proc. IEEE,* **63**: 1734–1737, 1975.
25. R. D. Graglia et al., Electromagnetic scattering for oblique incidence on impedance bodies of revolution, *IEEE Trans. Antennas Propag.,* **43** (1): 11–26, 1995.
26. M. W. Browne, "Two Rival Designers Led the Way to Stealthy Warplanes," in "The New York Times," Science Times Section, US, May 14, 1991.
27. S. F. Brown, "The Secret Ship," in magazine "Popular Science," US, October 1993.
28. B. Rich and L. Janos, *Skunk Works,* Boston-New York-London: Little, Brown & Company, 1994.
29. K. J. Vinoy and R. M. Jha, *Radar Absorbing Materials,* Boston: Kluwer Academic Publishers, 1996.

Reading List

This section contains short comments on some related references.

P. C. Fritch (ed.), *Radar Reflectivity,* Special issue of the *Proc. IEEE,* **53** (8), August 1965.

The first attempt to sum up basic results in the field of RCS. Includes a comprehensive subject index, about 1500 titles (pp. 1025–1064).

J. W. Crispin Jr. and K. M. Siegel (eds.), *Methods of Radar Cross Section Analysis.* New York: Academic Press, 1968.

Includes a short historical survey of high-frequency approximations. Contains results of such approximations for monostatic and bistatic RCS of simple objects. States a strategy of RCS calculations for complex objects. Some results are conveniently summarized in tables. Table 5 on p. 147 contains expressions for RCS in the Rayleigh region (for objects small in comparison with wavelength). High-frequency monostatic and bistatic RCS are given in Tables 7 and 8 on p. 168, 169, 171.

G. T. Ruck, D. E. Barrick, W. D. Stuart, and C. K. Kirchbaum, *Radar Cross-Section Handbook.* New York: Plenum Press, 1970.

This is a real encyclopedia of RCS, which includes most results obtained before 1970. It contains numerous theoretical and experimental results for both perfectly conducting and absorbing objects. The physical theory of diffraction (PTD) is mentioned here as the Sommerfeld–Macdonald technique. Equation (5.1-54), presented on p. 351, for the bistatic RCS of an ellipsoid is incorrect. In the particular case when an ellipsoid transforms into a sphere, this equation does not provide the bistatic RCS for the sphere, $\sigma = \pi a^2$. Instead it leads to the wrong quantity $\sigma = \pi a^2/(1 + \cos\beta)^2$, where β is the bistatic angle.

J. J. Bowman, T. B. A. Senior, and P. L. E. Uslenghi (eds.), *Electromagnetic and Acoustic Scattering by Simple Shapes.* New York: Hemisphere Publishing Corp., 1987.

Contains a comprehensive collection of theoretical results for RCS of simple objects which allow the exact solutions of diffraction problems. Both low-frequency and high-frequency approximations are presented as well.

M. Skolnik (ed.), *Radar Handbook.* New York: McGraw-Hill, 1970.

Contains many results of measurements and calculations for RCS. Calculations were carried out mostly by the physical optics approach and GTD. Analytical expressions for RCS are not given.

W. R. Stone (ed.), *Radar Cross Sections of Complex Objects,* Special issue of the *Proc. IEEE,* **77** (5), May 1989.

W. R. Stone (ed.), *Radar Cross Sections of Complex Objects,* Special issue of the *IEEE Trans. Antennas Propag.* **37** (5), May 1989.

These two references contain many theoretical results concerning RCS for complex objects (perfectly conducting objects with complex shapes and simple objects with complex boundary conditions).

W. R. Stone (ed.), *Radar Cross Sections of Complex Objects,* New York: IEEE Press, 1989.

This book consists of a collection of articles. It includes expanded versions of about half of the papers published in two previously mentioned special issues. It also contains papers written especially for this book and reprints of some earlier key papers.

J. M. Bernard, G. Pelosi, and P. Ya. Ufimtsev (eds.),, *Radar Cross Sections of Complex Objects,* Special issue of the French journal *Annales des Telecommunications,* **50** (5–6), May–June 1995. It is published in English with abstracts translated into French.

Contains the asymptotic analysis of RCS for higher-order curved surfaces, physical theory of slope diffraction, PO and PTD analysis of trihedral corner reflectors, a selective review of some numerical methods for electromagnetic scattering, and some other results.

The following three books contain additional information on RCS. They include concise descriptions of basic exact and approximate techniques for prediction of RCS, they introduce methods of RCS enhancement and reduction, and they contain a large number of calculated and measured data for RCS of many typical simple and complex objects. The books complement each other, with emphasis on different aspects in the field of RCS.

A. L. Maffett, *Topics for a Statistical Description of Radar Cross Section.* New York: John Wiley & Sons, 1989.

This book treats the subject of RCS with special emphasis on statistical aspects and applications. It reflects broad interests of the author: from historical background and perspective through analytical and numerical methods of RCS calculation and RCS measurements to elements of detection theory, investigation of anisotropic layers, and the inverse problem for anisotropic materials with diagonal permittivity and permeability tensors.

A. K. Bhattacharyya and D. L. Sengupta, *Radar Cross Section Analysis and Control.* Boston-London: Artech House, 1991.

The book concentrates its attention on deliberate changes of RCS (enhancement and reduction). It contains a useful table (p. 108) which represents in concise form the comparison of different methods available for RCS analysis, with discussion of their advantages, disadvantages, and possible applications. It also complements other books by inclusion of the Maluzhinets function, which plays a fundamental role in the theory of scattering by absorbing objects with sharp edges or with impedance discontinuities. The computer code for the calculation of this important function is provided in the appendix of the book.

E. F. Knott, J. F. Schaffer, and M. T. Tuley, *Radar Cross Section,* 2nd Ed. Boston-London: Artech House, 1993.

This book presents updated material which covers most aspects of RCS: radar fundamentals, radar detection, RCS prediction, RCS reduction, radar absorbing materials, and RCS measurements. Chapter 14 can be especially useful for a brief review. It contains a table (p. 562) with RCS estimations, as well as the RCS data presentation formats and data reduction recipes.

P. Ya. Ufimtsev, Comments on diffraction principles and limitations of RCS reduction techniques, *Proc. IEEE,* **84**: 1830–1851, 1996.

RCS reduction techniques are discussed briefly from the physical point of view. Attention is concentrated on the physical structure of radar waves scattered from large objects. Possible passive and active techniques to control and reduce reflected beams, rays, and shadow radiation as well as potential limitations of these techniques are considered. In particular, it is emphasized that grazing reflected rays and shadow radiation cannot be eliminated by absorbing materials.

R. C. Hansen (ed.), *Geometrical Theory of Diffraction.* New York: IEEE Press, 1981.

This book consists of a collection of articles. It contains key papers on GTD, asymptotic solutions of some canonical problems, and applications-oriented papers.

Many scattering objects contain nonmetallic materials, composites, and various layered structures. To simplify the solution of scattering problems for such objects, it is often practical to apply approximate boundary conditions. These conditions are enforced on the external surface of the object and contain important information about the internal structure of the scattering object. As a result, this approximation allows one to substantially reduce the spatial region under investigation. The two following books present the development and applications of this approximation technique.

T. B. A. Senior and J. L. Volakis, *Approximate Boundary Conditions in Electromagnetics.* London: The Institution of Electrical Engineering, 1995.

D. J. Hoppe and Y. Rahmat-Samii, *Impedance Boundary Conditions in Electromagnetics,* Washington, D.C.: Taylor & Francis, 1995.

PYOTR YA. UFIMTSEV
University of California
at Los Angeles

BACKSCATTERING. See BACKSCATTER.

(